Article

pubs.acs.org/Biomac

Toward Unimolecular Micelles with Tunable Dimensions Using Hyperbranched Dendritic-Linear Polymers

Christian Porsch,[†] Yuning Zhang,[‡] Cosimo Ducani,[§] Francisco Vilaplana,[∥,⊥] Lars Nordstierna,[#] Andreas M. Nyström,[‡] and Eva Malmström*,[†]

[†]School of Chemical Science and Engineering, Department of Fibre and Polymer Technology, KTH Royal Institute of Technology, SE-100 44 Stockholm, Sweden

[‡]IMM Institute of Environmental Medicine, Nanosafety & Nanomedicine Laboratory, Karolinska Institutet, SE-171 77 Stockholm, Sweden

[§]Swedish Medical Nanoscience Center, Department of Neuroscience, Karolinska Institutet, SE-171 77 Stockholm, Sweden

[∥]School of Biotechnology, Division of Glycoscience, KTH Royal Institute of Technology, SE-106 91 Stockholm, Sweden

[⊥]Wallenberg Wood Science Centre (WWSC), KTH Royal Institute of Technology, SE-100 44 Stockholm, Sweden

[#]Department of Chemical and Biological Engineering, Applied Surface Chemistry, Chalmers University of Technology, SE-412 96 Göteborg, Sweden

Supporting Information

ABSTRACT: A library of amphiphilic, hyperbranched dendritic-linear polymers (HBDLPs) are successfully synthesized, and evaluated as potential unimolecular micelles. Hyperbranched macroinitiators (HBMI), extended with poly(ethylene glycol) methacrylate (P(OEGMA)), are afforded via a combination of self-condensing vinyl (co)polymerization (SCV(C)P) and atom transfer radical polymerization (ATRP), providing a versatile two-step synthetic route. The HBDLP architecture and chain lengths are varied, and the effect on the nanoparticle (NP) stability and properties are evaluated. The HBDLPs form predominantly stable and spherical NPs, and the NP dimensions could be tailored by the HBDLP characteristics. The NPs formed are of high molecular weight, and their stability varies with the properties of the corresponding HBDLP. Too small dendritic segment, or too low degree of PEGylation, results to some extent in NP aggregation, while higher molecular weight HBDLPs, with a high amount of hydrophilic segments, appears to form discrete unimolecular micelles. The versatility of the platform is further demonstrated by the convenience of forming a HBDLP with a more complex, linear copolymer extension instead of P(OEGMA).

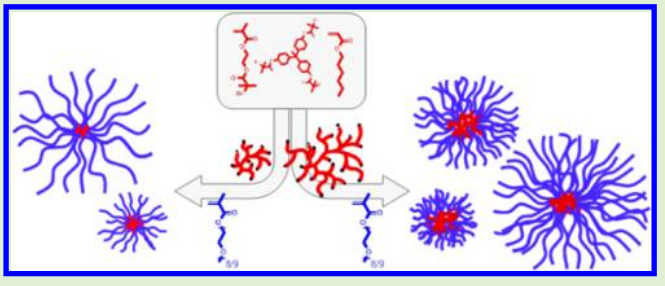

INTRODUCTION

The progress in polymer chemistry has provided researchers worldwide with the possibility to tune the architecture and functionality of polymers in the search for more sophisticated nanostructured materials. In the past decades, the interest for improved and more personalized medicine has challenged researchers to design delivery platforms for pharmaceuticals, and chemotherapeutics in particular.[1] Polymer nanoparticles (NPs), displaying a core−shell morphology, have shown great potential as therapeutic delivery systems, due to their demonstrated ability to enhance the solubility, bioavailability, circulation time, and selective localization of small molecular therapeutics.[2−4] Traditionally, polymer micelles, as well as other polymer morphologies at the nanoscale, have been formed via self-assembly of amphiphilic linear block copolymers,[5−7] and Wooley et al.[8] have shown that such assemblies can be stabilized by shell cross-linking to avoid the drawbacks with micelle instability below the critical micelle concentration. Furthermore, as an alternative to linear polymers, the relatively high solubility and numerous end-group functionality of dendritic polymers[9] (dendrimers/dendrons, hyperbranched polymers, and dendritic-linear polymers (DLPs)) have attracted significant attention for the design of nanoparticles with applicability as therapeutic delivery systems.[10−16] While the elaborate synthesis of dendrimers may hamper their applicability, the less complicated and less time-consuming preparation of hyperbranched polymers make them particularly attractive for the synthesis of stable amphiphilic macromolecules.[11]

Already in 1952, Flory[17] postulated the stepwise synthesis of highly branched polymers using AB_x-type ($x \geq 2$) building blocks, however; it took until 1995 before Fréchet et al.[18] reported the first radical polymerization of AB*-type monomers, referred to as self-condensing vinyl polymerization (SCVP), to produce hyperbranched polymers. The consecutive development of controlled radical polymerization (CRP) techniques, including atom transfer radical polymerization (ATRP)[19,20] and reversible

Received: March 7, 2014
Revised: April 29, 2014
Published: May 2, 2014

dx.doi.org/10.1021/bm5003637 | Biomacromolecules 2014, 15, 2235−2245

addition-fragmentation chain transfer (RAFT),[21] further revolutionized the synthesis of hyperbranched polymers based on vinyl monomers, and popular approaches previously reported are copolymerization of monovinyl monomers with small amounts of divinyl monomers,[22−24] or the above-mentioned SCVP approach.[25−28] SCVP utilizes inimers, which are AB*-type initiator monomers where A is a vinyl group, and B a pendant group, which can be converted into an initiating species, and thereby introduce branches to the polymer backbone. One advantage of SCVP is that it possesses the same versatility as conventional CRP techniques, thus providing the possibility to copolymerize an inimer with essentially any monomer having vinyl functionality. Consequently, by employing self-condensing vinyl (co)polymerization (SCV(C)P), a wide range of commercially available comonomers can be utilized to introduce function to and/or tailor the degree of branching of the polymer.[29,30] In addition, the use of a controlled polymerization technique, such as ATRP, enables subsequent chain-extension of the branched polymer with linear segments. This offers a versatile synthesis of complex hyperbranched DLPs, which may be a promising approach to generate amphiphilic nanoscopic objects. Further, it has been proposed that the intrinsic three-dimensional integrity of such amphiphilic DLPs ideally may result in unimolecular micelles,[11,31−33] and offer significant stability in comparison to traditional block copolymer assemblies.

Our group has an interest in employing advanced macromolecular synthesis to design polymer amphiphiles of various architectures.[34−42] One key area of specific interest is the assembly of such polymers into NPs and their applicability to serve as drug delivery systems, or for the construction of dual-function devices, combining therapeutic delivery with diagnostic readouts—theranostics—to combat cancer, typically evaluated in breast cancer models.[43−47] PEGylation has for a long time been known as an effective approach to provide NPs carriers with high water solubility and nonfouling properties, thus enabling enhanced circulation time.[3,4] In the past decade, oligo(ethylene glycol) methacrylates (OEGMAs) have emerged as an interesting alternative to linear PEGylation.[48,49] Since OEGMAs are feasible to polymerize via CRP techniques, they offer a facile synthesis, and a high degree of structural freedom as they can be copolymerized with other vinyl monomers to introduce additional functionality to the polymer. In this work we are exploring the synthesis of PEG end-capped, high molecular weight HBDLPs in a two-step procedure via the combination of SCV(C)P and ATRP. We are further demonstrating the ability of these complex polymers to form unimolecular micelles in aqueous solution, and the possibility to tailor the micelle size by the composition of the HBDLPs. In addition, the versatility of the HBDLP platform is further demonstrated through the facile introduction of functional fluorine-containing monomers to the NP exterior. As reported previously, such ^{19}F-containing NPs have potential as theranostic delivery platforms.[43,50,51]

EXPERIMENTAL SECTION

Reagents and Materials. 2-Hydroxyethyl methacrylate (HEMA, >99%), 4-(dimethylamino)pyridine (DMAP, 99%), 2-bromisobutyryl bromide (BiB, 98%), 1,1,1-tris(4-hydroxyphenyl)ethane (THPE, 99%), 2,2-bipyridyl (bipy, >99%), copper(I) chloride (Cu(I)Cl, >99%), copper(II) chloride ($Cu(II)Cl_2$, 97%), copper(II) bromide ($Cu(II)Br_2$, 99%), trifluoroacetic acid (TFA, 99%), ethylenediaminetetraacetic acid disodium salt dehydrate (EDTA, >99%), penicillin−streptomycin solution, sodium dodecyl sulfate (SDS), (3-(4,5-dimethylthiazol-2-yl))-2,5-diphenyl tetrazolium bromide (MTT), formaldehyde solution, and phosphate buffered saline (PBS) were purchased from Sigma-Aldrich. Triethylamine (TEA, >99%) was purchased from Merck. Oligo(ethylene glycol) methyl ether methacrylate (OEGMA, average M_w 475 g mol^{-1}, Aldrich), *tert*-butyl methacrylate (*t*-BMA, M_w 142 g mol^{-1}, Aldrich), and hexyl acrylate (HA, M_w 130 g mol^{-1}, Aldrich) were activated by passage through a column of neutral aluminum oxide prior to use. Trifluoroethyl methacrylate (TFEMA, M_w 168 g mol^{-1}, Aldrich) was used as received. Human breast cancer cell lines, MCF-7, MDA-MB-231, and MDA-MB-468, were purchased from the American Type Culture Collection (ATCC), and mouse macrophage cell line RAW 264.7 was kindly supplied by Professor Richter-Dahlfors at Karolinska Institutet (Stockholm, Sweden). Cell lines were maintained in Dulbecco's Modified Eagle Medium (DMEM) supplemented with 10% (v/v) fetal bovine serum (FBS), 100 U/mL penicillin, and 100 mg mL^{-1} streptomycin, and incubated at 37 °C with 5% CO_2. FBS was purchased from Hyclone Laboratories. 4′,6-Diamidino-2-phenylindole (DAPI) was obtained from Molecular Probes. All other chemicals were purchased from conventional suppliers and used as received.

Methods. *Nuclear Magnetic Resonance (NMR).* ^{1}H-, ^{13}C-, and ^{19}F-NMR (1D) spectra for structure analysis were recorded on a Bruker Avance AM 400 NMR instrument using $CDCl_3$, $(CD_3)_2SO$, or D_2O as solvent. The residual solvent peak was used as the internal standard if nothing else is stated.

^{1}H NMR Diffusion. Diffusion measurements were carried out on a Bruker Avance 600 spectrometer, equipped with a diffusion probe with a maximum gradient strength of 1200 G/cm. Using the conventional stimulated-echo sequence,[52] the diffusion experiments were performed at 25 °C with diffusion time Δ = 100 ms, gradient pulse length δ = 0.5 ms, and the gradient strength linearly ramped in 16 steps from g = 0 to 1200 G/cm. The time parameters in this setup generated a minimal loss of signal intensity introduced by longitudinal and transverse relaxation during the pulse sequence. At each gradient step, a 1.66 ms spoiler gradient of −20 G/cm was applied, and 16 acquisitions were collected to acquire the ^{1}H spectrum. The relaxation delay was set to 5 s to ensure full longitudinal relaxation. Correct calibration of the gradient amplifier was controlled by obtaining the self-diffusion coefficient of HDO trace in a standard sample of pure D_2O.[53] Calculation of the self-diffusion coefficient distribution was done by fitting a distribution model by standard nonlinear regression of the decay of signal integral intensity. Here the general Schulz distribution equation was selected,[54] which contains a simple numeric solution to the inverse Laplace transform. The mean value and standard deviation of the given distribution were calculated, and the diffusion distribution was recalculated to picture the molecular diameter distribution through the Stokes−Einstein equation. Here we should stress that the shape and low concentration of the molecules allowed the classical model of infinite dilution of spheres with stick boundary conditions. Two signals of high signal intensity, at 3.7 and 3.4 ppm, respectively, were selected for diffusion processing. Diameter distributions of all samples can be found in the Supporting Information (Figure S5). Table 2 gives the average mean diameter and standard deviation calculated from the average of two distributions for each sample except for HBDLP-1, where experimental noise did not allow accurate regression analyses for the signal at 3.4 ppm.

Size Exclusion Chromatography (SEC). SEC measurements were performed on a TOSOH EcoSEC HLC-8320GPC system equipped with an EcoSEC RI detector and three columns (PSS PFG 5 μm; Micro-guard, 100 Å, and 300 Å) (MW resolving range: 100−300 000 g mol^{-1}) from PSS GmbH, using DMF (0.2 mL min^{-1}) with 0.01 M LiBr as the mobile phase at 50 °C. A conventional calibration method was created using narrow poly(methyl methacrylate) standards ranging from 700 to 2 000 000 g mol^{-1}, and used to determine the average molar masses (number-average molar mass, M_n, and weight-average molar mass, M_w) and the dispersity ($Đ_M = M_w/M_n$). Corrections for flow rate fluctuations were made using toluene as an internal standard. PSS WinGPC Unity software, version 7.2, was used to process the data.

Size Exclusion Chromatography−Multiple Angle Laser Light Scattering (SEC-MALLS). Absolute molar mass determinations were performed by size exclusion chromatography (SEC, SECcurity 1260, PSS, Mainz, Germany) coupled to a multiple angle laser light scattering detector (MALLS, BIC-M_wA7000, Brookhaven Instrument Corp., New York) and a refractive index detector (SECcurity 1260, PSS,

Mainz, Germany) thermostated at 40 °C. Separations were performed using a combined column setup with a SUPREMA precolumn, a SUPREMA 1000 Å, and two SUPREMA 3000 Å analytical columns (PSS, Mainz, Germany) with 1 mL min^{-1} of H_2O (10 mM NaOH) as the mobile phase at 40 °C. Calibration of the detectors and the column setup was performed by injection of pullulan standards (PSS, Mainz, Germany). Prior to analysis, all samples were dissolved in H_2O (10 mM NaOH) overnight at room temperature. The differential index of refraction (d*n*/d*c*) of the polymers was calculated by repeated injection of 100 μL at five different concentrations between 0.2 and 5 g L^{-1}. Data collection and analysis from SEC separations with light scattering detection was performed using WinGPC software (PSS, Mainz, Germany).

Dynamic Light Scattering (DLS). Samples were analyzed with a Malvern Zetasizer NanoZS at 25 °C in PBS using polymer concentrations of 1.25 mg mL^{-1}. Prior to the measurements, all samples were filtered through a 0.45 μm nylon filter to remove dust particles, and allowed to equilibrate for 5 min. Measurements were also conducted on unfiltered samples to ensure that no polymer particles were removed by the filtration. All results are averages of four individual samples where the mean size is an average of 10 measurements for each sample.

Transmission Electron Microscopy (TEM). Three μL of NP solution (10 mg mL^{-1} in PBS (50 μg mL^{-1} for HBDLP-6)) was placed on a glow-discharged, carbon-coated Formvar grid (Electron Microscopy Sciences) and incubated for 20 s. The drop was removed with filter paper, and the procedure was repeated 4 times to ensure a high concentration of particles on the grid. Subsequently, the sample was stained with 2% (w/v) aqueous uranyl formate solution for 20 s. TEM images were obtained with a FEI Morgagni 268(D) Transmission Electron Microscope at 80 kV at magnifications 16 000−22 000.

Cell Viability Tests. MTT assay was selected to evaluate mitochondria function. Breast cancer cells, MCF-7, MDA-MB-231, and MDA-MB-468 were harvested by trypsin and RAW 264.7 via physical scraping. Cells were washed with PBS, resuspended in DMEM medium, and seeded into 96 well plates at a concentration of 1×10^4 cells per well (1×10^5 cell mL^{-1}, 100 μL) and precultured for 24 h. For the pure NP toxicity assays, all four cell lines were included. Cells were incubated in fresh medium containing the different polymers with designed concentrations (0.01, 0.1, 1, 10, and 100 μg mL^{-1}) separately for 72 h. For the DOX-NPs efficacy assay, only the MDA-MB-468 cell line was selected and treated with free DOX and different DOX-NPs at designed drug concentrations (0.01, 0.1, 1, 5 and 10 μg mL^{-1}) for 48 h. For both pure NPs and DOX-NP experiments, five parallel wells were set for each concentration. Ten microliters (5 mg mL^{-1}) of MTT was introduced into each well after incubation, and after additional 4 h, 100 μL of 10% SDS solution was added. Absorbance readings at 570 nm wavelengths were obtained with a BioTek Synergy MX plate reader 18 h later.

Doxorubicin Loading. A DOX stock solution was prepared by dissolving DOX and TEA (1:3 mol eq) in CH_2Cl_2 (1 mg mL^{-1}). The stock solution (1 mL) was diluted with CH_2Cl_2 (1 mL) and mixed with a PBS solution of NPs (4 mL, 1.25 mg mL^{-1}). The mixture was stirred overnight at 100 rpm in order to evaporate the organic solvent. Free DOX was removed by spin filtration with a MWCO of 3 kDa by refilling PBS every 5 min. The concentration of DOX in the NPs was measured by comparing UV absorbance at 490 nm, of samples diluted with DMF:H_2O (4:1) to a standard curve (five replicates).

In Vitro Drug Release. Free DOX or DOX-NPs solutions were transferred into 3 mL dialysis cassettes (MWCO 3500, Slide-A-Lyzer, Thermo) suspended in 4 L of PBS at 37 °C. Samples inside cassettes were collected (triplicates of 10 μL each) at the following time intervals: 0, 2, 4, 8, 12, 24, 48, and 72 h, and transferred into black 96-well plates, containing 100 μL DMF:H_2O (4:1) in each well. The fluorescence intensity of each well was determined with a BioTek Synergy MX plate reader at the wavelength 480/600 (excitation/emission) nm.[44]

DOX Internalization Studies. MDA-MB-468 cells were seeded onto the coverslips placed in the bottom of six-well plates at a density of 5×10^5 cells per well and incubated for 24 h. The cells were incubated with 5 μg mL^{-1} DOX or DOX-NPs for 2, 4, or 24 h. The cells were fixed with 4% formaldehyde and stained with DAPI (2.5 μg mL^{-1}, 15 min). After washing with PBS 3 times, the coverslips were embedded on glass slides and observed via a confocal microscope (META LSM510 Zeiss) with 40x OilDIC objective at the following settings: DAPI was excited with the 405 nm laser and fluorescence collected after a BP420/480 filter; DOX was excited with the 543 nm laser and fluorescence collected after a BP560/615 filter. Image data were acquired with LSM software and analyzed with ImageJ.

Preparation of Nanoparticles. To form stable NPs in aqueous solution, the following procedure was employed: the polymer was completely dissolved in CH_2Cl_2 (2 mL, 1.25 mg mL^{-1}) in a glass vial stirred at 200 rpm by a magnetic stirrer. PBS (2 mL) was then added using a syringe pump over a time period of 2 h. CH_2Cl_2 was allowed to evaporate overnight to achieve the stable NPs in PBS solution at a final concentration of 1.25 mg mL^{-1}. In addition, NPs formed by direct dissolution in PBS for 4 days were also analyzed by DLS to corroborate a successful NP formation with the above-mentioned procedure.

Syntheses. *Synthesis of the Trifunctional ATRP Initiator 1,1,1-Tris(4-(2-bromoisobutyryloxy)phenyl)ethane (TBBPE).* The synthesis of the trifunctional ATRP initiator, TBBPE, was adopted from a procedure reported by Matyjaszewski et al.[55] BiB (33.1 g, 0.144 mol) was dissolved in tetrahydrofuran (THF, 250 mL) in a 500 mL three-necked round-bottom flask equipped with a magnetic stirrer, and cooled to 0 °C on an ice/water bath. THPE (11.0 g, 35.9 mmol) and TEA (21.8 g, 0.215 mol) were dissolved in THF (200 mL), and slowly added to the reaction mixture under argon flow. The reaction mixture was allowed to warm up to room temperature and stirred overnight. The formed salts were removed by filtration, and THF was removed by rotary evaporation. The product was redissolved in ethyl acetate (EtOAc, 600 mL) and extracted with 3 × 100 mL NaOH (aq, 5 wt %) and 1 × 100 mL H_2O. The organic phase was dried over magnesium sulfate ($MgSO_4$), filtered, and concentrated under reduced pressure. The pure product was afforded as a white powder in 48% yield after two recrystallizations from EtOAc. ^{1}H NMR (400 MHz, $CDCl_3$): δ 2.07 (s, 18H, $-CH_3$), 2.19 (s, 3H, $-CH_3$), 7.07 (q, 12H, *J* = 8.7 Hz, −Ar−) ppm. ^{13}C NMR ($CDCl_3$): δ 30.69, 51.75, 55.47, 120.55, 129.78, 146.40, 149.09, 170.26 ppm.

Synthesis of the Inimer 2-(2-Bromoisobutyryloxy)ethyl Methacrylate (BBEMA). The inimer was synthesized employing a one-step esterification reaction between BiB and HEMA. HEMA (20.0 g, 0.154 mol), pyridine (14.9 mL, 0.185 mol), and DMAP (3.76 g, 30.8 mmol) were dissolved in CH_2Cl_2 (100 mL) in a round-bottom flask immersed in a 0 °C ice/water bath. BiB (22.9 mL, 0.185 mol) was dissolved in CH_2Cl_2 (100 mL), and slowly added to the reaction mixture. The reaction mixture was allowed to warm up to room temperature and stirred overnight. The remaining BiB was quenched with 50 mL of H_2O, and the mixture was stirred for 1 h. The reaction mixture was diluted with an additional 300 mL of CH_2Cl_2 and extracted with 3 × 100 mL $NaHSO_4$ (aq. 10 wt %), 3 × 100 mL Na_2CO_3 (aq. 10 wt %), and 1 × 100 mL brine. The organic phase was dried over $MgSO_4$, filtered, and concentrated under vacuum. The pure product was achieved as a viscous liquid by liquid column chromatography on silica gel, eluting with heptane:EtOAc mixtures. Yield: 85%. ^{1}H NMR (400 MHz, $CDCl_3$): δ 1.90 (s, 6H, $-CH_3$), 1.91 (s, 3H, $-CH_3$), 4.43 (m, 4H, $-CH_2-$), 5.60 (s, 1H, −CH), 6.15 (s, 1H, −CH) ppm. ^{13}C NMR ($CDCl_3$): δ 18.78, 31.17, 55.85, 62.41, 64.02, 126.70, 136.34, 167.52, 171.95 ppm.

General Procedure for Polymerization of Hyperbranched Macroinitiator HBMI(TBBPE-co-BBEMA-co-HA) via ATRP (Scheme 1, HBMI-1 and HBMI-2). The two different hyperbranched macroinitiators (HBMI-1 and HBMI-2) were synthesized by employing SCV(C)P under ATRP conditions. In a typical experiment (HBMI-1), TBBPE (0.300 g, 0.398 mmol) was completely dissolved in anisole (70 wt % with respect to monomer) in a round-bottom flask equipped with a magnetic stirrer. Bipy (411 mg, 2.63 mmol), HA (1.98 g, 12.7 mmol), and BBEMA (890 mg, 3.19 mmol) were added and allowed to mix. The flask was sealed with a rubber septum, cooled to 0 °C on an ice/water-bath, and evacuated/backfilled with argon (5 + 5 min). Cu(I)Cl (118 mg, 1.19 mmol) and Cu(II)Cl_2 (16.1 mg, 120 μmol) were quickly added under argon flow, followed by two additional vacuum/argon cycles.

Scheme 1. Schematic Illustration of the Synthetic Route to the Hyperbranched Dendritic-Linear Polymers via Initially SCV(C)P-ATRP and Subsequently ATRP Polymerization Techniques[a]

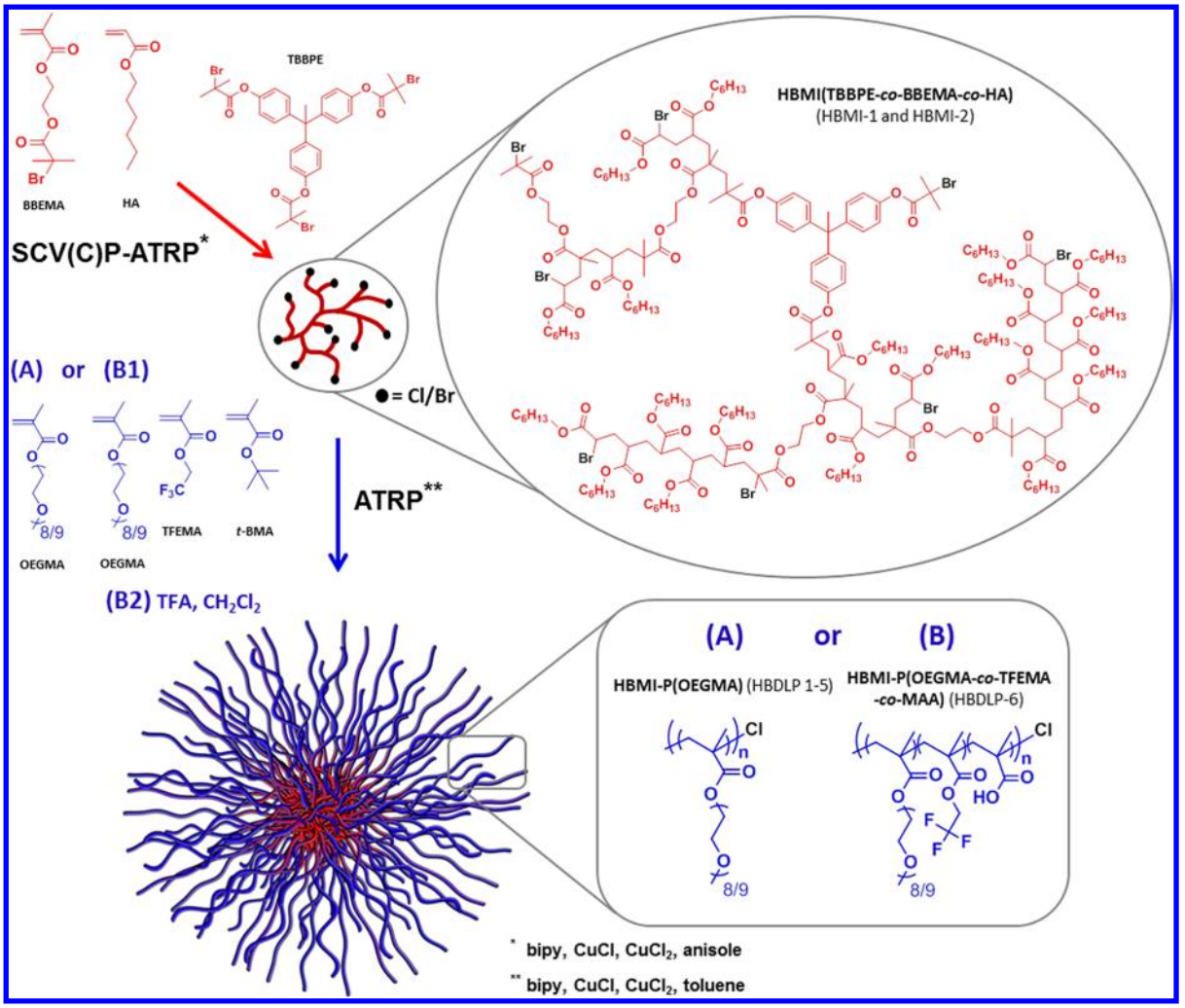

[a]The schematic representation of the HBMI is one of several potential structures.

Table 1. Molecular Properties of the Synthesized Hyperbranched Macroinitiators (HBMI)

polymer[a]	feed ratio TBBPE:BBEMA:HA	polymer ratio[b] TBBPE:BBEMA:HA	$M_{n,\,NMR}$[b] (g mol^{-1})	$M_{n,\,SEC}$[c] (g mol^{-1})	$Đ_M$[c]	Br/mol[d]
HBMI-1	1:8:32	1:12:37	10 000	3 600	1.3	15
HBMI-2	1:60:240	1:51:295	61 000	6 100	1.5	54

[a]Full name: HBMI(TBBPE-*co*-BBEMA-*co*-HA). [b]Assessed from ^{1}H NMR ($CDCl_3$) assuming one TBBPE-moiety per HBMI. [c]Apparent number-average molecular weight determined by DMF-SEC calibrated with linear PMMA standards. [d]Average calculated from ^{1}H NMR assuming one TBBPE-moiety per HBMI and high end-group fidelity.

The reaction was started by immersing the flask into an oil-bath preheated to 60 °C, its progress followed by ^{1}H NMR, and allowed to proceed to high conversion (>95%). To preserve the end-groups, the reaction was terminated by the addition of Cu(II)Br_2 (266 mg, 1.19 mmol) and stirred for 10 min at reduced pressure. The flask was removed from the oil-bath to stop the reaction, and the content exposed to air, whereafter the reaction mixture was heavily diluted with CH_2Cl_2. The copper complex was removed by passing the reaction mixture through a short plug of neutral aluminum oxide before all solvents were removed under reduced pressure. The product was collected as a viscous liquid after three precipitations in an excess of cold methanol from THF, sedimentation, and decantation. HBMI-1 (Table 1) was synthesized with the following molar ratios of reagents: [TBBPE]:[HA]:[BBEMA]:[bipy]:[Cu(I)Cl]:[Cu(II)Cl_2] = [1]:[32]:[8]:[6.6]:[3]:[0.3], while for HBMI-2 (Table 1) the [TBBPE]:[HA]:[BBEMA] ratio was changed to [1]:[240]:[60]. ^{1}H NMR (400 MHz, $CDCl_3$): δ 0.9 (br, s, $-CH_3$ from HA), 1.1–1.2 (br, m, –CH and $-CH_3$ from backbone), 1.3 (br, s, $-CH_2-$ from HA), 1.6 (br, s, $-CH_2-$ from HA), 1.8–2.8 (br, m, $-CH_2-$ from backbone and $-CH_3$ from initiating moieties), 4.0–4.4 (br, m, $-COO-CH_2-$ from BBEMA and HA), 6.9–7.2 (br, m, –Ar– from TBBPE) ppm.

General Procedure for Chain-Extension with P(OEGMA) from the Hyperbranched Macroinitiators via ATRP (HBDLP 1–5, Scheme 1, Path A). The active chain-ends on the HBMIs (HBMI-1 and HBMI-2) were chain-extended with the monomer OEGMA employing ATRP. To synthesize HBDLPs 1–5 (Table 2), the following molar ratios of reagents were used: [HBMI]:[OEGMA]:[bipy]:[Cu(I)Cl]:[Cu(II)Cl_2] = [1]:[n]:[6.6]:[3]:[0.3], where n was varied between 10 and 200 depending of the targeted degree of polymerization. In a typical experiment (HBDLP-2), HBMI-1 (100.0 mg, approximately 152 μmol of Br) was completely dissolved in toluene (70 wt % with respect to monomer) in a round-bottom flask equipped with a magnetic stirrer. Bipy (156 mg,

dx.doi.org/10.1021/bm5003637 | Biomacromolecules 2014, 15, 2235–2245

0.987 mmol) and OEGMA (14.4 g, 30.3 mmol) were added and allowed to mix. The flask was sealed with a rubber septum, cooled to 0 °C on an ice/water-bath, and evacuated/backfilled with argon (10 + 10 min). Cu(I)Cl (45.0 mg, 455 μmol) and $Cu(II)Cl_2$ (6.1 mg, 46 μmol) were quickly added under argon flow followed by two additional vacuum/argon cycles. The reaction was started by immersion into an oil-bath preheated to 60 °C, its progress followed by ^1H NMR, and allowed to proceed to roughly 50% conversion. The flask was removed from the oil-bath to stop the reaction, and the content exposed to air, whereafter the reaction mixture was heavily diluted with CH_2Cl_2. The copper complex was removed by passing the reaction mixture through a short plug of neutral aluminum oxide before all solvents were removed at reduced pressure. The product was purified by two precipitations in an excess of cold diethyl ether from THF. Thereafter, to remove potentially remaining copper, the product was dissolved in deionized (DI) water, charged into a dialysis tube (MWCO 6−8000), and dialyzed against DI water for 12 h, EDTA solution (aq. 5 wt %) for 8 h, and finally DI water again for 12 h. The dialysis medium was changed regularly. The final product was isolated as a viscous liquid by lyophilization. ^1H NMR (400 MHz, $(CD_3)_2SO$): δ 0.6−1.0 (br, m, $-CH_3$ from HA in HBMI and P(OEGMA) backbone), 1.3 (br, s, $-CH_2-$ from HA in HBMI), 1.5 (br, s, $-CH_2-$ from HA in HBMI), 1.5−2.0 (br, m, $-CH_2-$ from P(OEGMA) backbone), 3.3 (br, s, $-O-CH_3$ from P(OEGMA) side chain), 3.4−3.7 (br, m, $-CH_2-$ from P(OEGMA) side chain), 3.9−4.3 (br, m, $-COO-CH_2-$ from P(OEGMA) side chain and HBMI) ppm.

Chain-Extension with P(OEGMA-co-TFEMA-co-tBMA) from the Hyperbranched Macroinitiators via ATRP (Scheme 1, Path B1). The active chain-ends on HBMI-2 were chain-extended with the monomers OEGMA, TFEMA, and *t*-BMA employing ATRP. To synthesize HBDLP-6 (Table 2), the following molar ratios of reagents were used: [HBMI-2]:[OEGMA]:[TFEMA]:[*t*-BMA]:[bipy]:[Cu(I)Cl]:[$Cu(II)Cl_2$] = [1]:[55]:[110]:[55]:[6.6]:[3]:[0.3]. HBMI-2 (200.0 mg, 177.1 μmol of Br) was completely dissolved in toluene (70 wt % with respect to monomer) in a round-bottom flask equipped with a magnetic stirrer. Bipy (210 mg, 1.34 mmol), OEGMA (4.63 g, 9.74 mmol), TFEMA (3.76 g, 15.9 mmol), and *t*-BMA (1.39, 9.74 mmol) were added and allowed to mix. The flask was sealed with a rubber septum, cooled to 0 °C on an ice/water-bath, and evacuated/backfilled with argon (10 + 10 min). Cu(I)Cl (52.5 mg, 530 μmol) and $Cu(II)Cl_2$ (7.2 mg, 53.0 μmol) were quickly added under argon flow followed by two additional vacuum/argon cycles. The reaction was started by immersing the flask into an oil-bath preheated to 60 °C, and its progress was followed by ^1H NMR. The reaction was allowed to proceed to approximately 25% conversion. The flask was removed from the oil-bath to stop the reaction, and the content exposed to air, whereafter the reaction mixture was heavily diluted with CH_2Cl_2. The copper complex was removed by passing the reaction mixture through a short plug of neutral aluminum oxide before all solvents were removed under reduced pressure. The product was purified by three precipitations in an excess of cold heptane from THF, and collected as a white solid. Trace amounts of hydrophilic OEGMA monomer remained in the product; however, the purification procedure during the following deprotection step to form HBDLP-6 resulted in its removal. ^1H NMR (400 MHz, $CDCl_3$) after three precipitations: δ 0.6−1.1 (br, m, $-CH_3$ from HA in HBMI and P(OEGMA-*co*-TFEMA-*co*-*t*BMA) backbone), 1.3 (br, s, $-CH_2-$ from HA in HBMI), 1.4 (br, s, $-CH_3$ from P(OEGMA-*co*-TFEMA-*co*-**tBMA**)), 1.6 (br, s, $-CH_2-$ from HA in HBMI), 1.7−2.1 (br, m, $-CH_2-$ from P(OEGMA-*co*-TFEMA-*co*-*t*BMA) backbone and $-CH_3$ from OEGMA monomer), 3.3−3.8 (br, m, $-O-CH_3$ and $-CH_2-$ from P(**OEGMA**-*co*-TFEMA-*co*-*t*BMA) and OEGMA monomer side chain), 3.9−4.2 (br, m, $-COO-CH_2-$ from P(**OEGMA**-*co*-TFEMA-*co*-*t*BMA) side chain and HBMI), 4.2−4.5 (br, m, $-COO-CH_2-$ from P(OEGMA-*co*-**TFEMA**-*co*-MAA) side chain and OEGMA monomer), 5.6 and 6.1 (s, vinyl protons from OEGMA monomer) ppm.

Preparation of HBMI-P(OEGMA-co-TFEMA-co-MAA) by Acidolysis of the tert-Butyl Groups of HBMI-P(OEGMA-co-TFEMA-co-tBMA) (HBDLP-6, Scheme 1, Path B2). To synthesize HBDLP-6, a facile procedure using TFA was employed to remove the *tert*-butyl groups of HBMI-P(OEGMA-*co*-TFEMA-*co*-*t*BMA) to form methacrylic acid (MAA) residues. The deprotection was conducted by dissolving HBMI-P(OEGMA-*co*-TFEMA-*co*-*t*BMA) (1.5 g, ∼29 μmol of *t*-BMA by NMR) in CH_2Cl_2 (25 mL) in a round-bottom flask equipped with a magnetic stirrer. TFA (7.0 mL, 91 mmol) was added dropwise, and the reaction was allowed to proceed overnight under vigorous stirring in an open-air system. All remaining solvent was evaporated under reduced pressure, the product was redissolved in a THF/H_2O mixture (20 mL, 50/50 by volume), and charged into a dialysis tube (MWCO 6−8000). The product was purified by dialysis against DI water for 12 h, EDTA solution (aq. 5 wt %) for 8 h, and finally DI water again for 12 h. The dialysis medium was changed regularly, and the product was isolated as a white solid after lyophilization, and stored under argon atmosphere at −20 °C. ^1H NMR (400 MHz, $(CD_3)_2SO$): δ 0.6−1.1 (br, m, $-CH_3$ from HA in HBMI and P(OEGMA-*co*-TFEMA-*co*-MAA) backbone), 1.3 (br, s, $-CH_2-$ from HA in HBMI), 1.5 (br, s, $-CH_2-$ from HA in HBMI), 1.6−2.1 (br, m, $-CH_2-$ from P(OEGMA-*co*-TFEMA-*co*-MAA) backbone), 3.3 (br, s, $-O-CH_3$ from P(**OEGMA**-*co*-TFEMA-*co*-MAA) side chain), 3.4−3.7 (br, m, $-CH_2-$ from P(**OEGMA**-*co*-TFEMA-*co*-MAA) side chain), 3.8−4.2 (br, m, $-COO-CH_2-$ from P(**OEGMA**-*co*-TFEMA-*co*-MAA) side chain and HBMI), 4.5−4.8 (br, m, $-COO-CH_2-$ from P(OEGMA-*co*-**TFEMA**-*co*-MAA) side chain), 12.2−13.0 (br, s, COOH from P(OEGMA-*co*-TFEMA-*co*-**MAA**)) ppm. ^{19}F-NMR (D_2O): 2.15 relative TFA (br, s, $-CF_3-$ of P(OEGMA-*co*-**TFEMA**-*co*-MAA)) ppm.

RESULTS AND DISCUSSION

In this work, a facile method to synthesize high molecular weight HBDLPs is described, employing a two-step procedure. Initially, hydrophobic HBMIs are produced employing SCV(C)P via ATRP. Subsequently, the active end-groups are exploited to chain-extend these hyperbranched polymers with hydrophilic linear polymers forming high molecular weight, amphiphilic, HBDLPs. The synthesized polymers are further utilized to form core−shell type NPs, and the influence of architecture and molecular weight on the NP characteristics is evaluated in detail, including a preliminary biological evaluation.

Synthesis of Hyperbranched Macroinitiators (HBMI). SCV(C)P has shown to be a viable approach to synthesize hyperbranched macromolecules by employing CRP techniques. This synthetic route makes use of inimers; molecules consisting of both a monomer and an initiator functionality, which under the suitable conditions polymerizes and form highly branched polymers.[18] In the present work we utilized the inimer, 2-(2-bromoisobutyryloxy)ethyl methacrylate (BBEMA),[56] together with the comonomer hexyl acrylate (HA), to synthesize HBMIs, as schematically illustrated in Scheme 1. BBEMA will bring about branching of the polymer while the aliphatic side chain of HA introduces hydrophobicity, which could favor effective loading of low molecular weight guest molecules, including therapeutics. Further, in order to reduce the molecular weight dispersity of the polymers, a trifunctional ATRP-initiator, 1,1,1-tris(4-(2-bromoisobutyryloxy)phenyl)-ethane (TBBPE), was synthesized according to the literature,[55] and utilized in small amounts. As shown by Pan et al.[57] the introduction of a multifunctional initiating moiety is an effective approach to reduce the molecular weight distribution of polymers obtained by SCVP.

By employing SCV(C)P-ATRP, different HBMIs were synthesized and their characteristics evaluated by ^1H NMR and SEC (Table 1, HBMI-1 and HBMI-2). The polymerizations were conducted in dilute anisole solutions, mediated by a 2,2-bipyridyl/Cu(I)Cl/$Cu(II)Cl_2$ system, and were allowed to proceed to high conversions (>95%). High conversion will favor high molecular weight since SCV(C)P proceeds partially via stepwise reaction kinetics.[18] To preserve a high proportion of active end-groups of the macroinitiators, the reactions were terminated by adding $Cu(II)Br_2$ under reduced pressure.

dx.doi.org/10.1021/bm5003637 | Biomacromolecules 2014, 15, 2235−2245

Two HBMIs with different molecular weights were synthesized by varying the initial [TBBPE]/([HA] + [BBEMA]) ratio while keeping [HA]/[BBEMA] constant. A typical ^{1}H NMR ($CDCl_3$) of HBMI-2 in $CDCl_3$ is shown in Figure 1A. Characteristic peaks

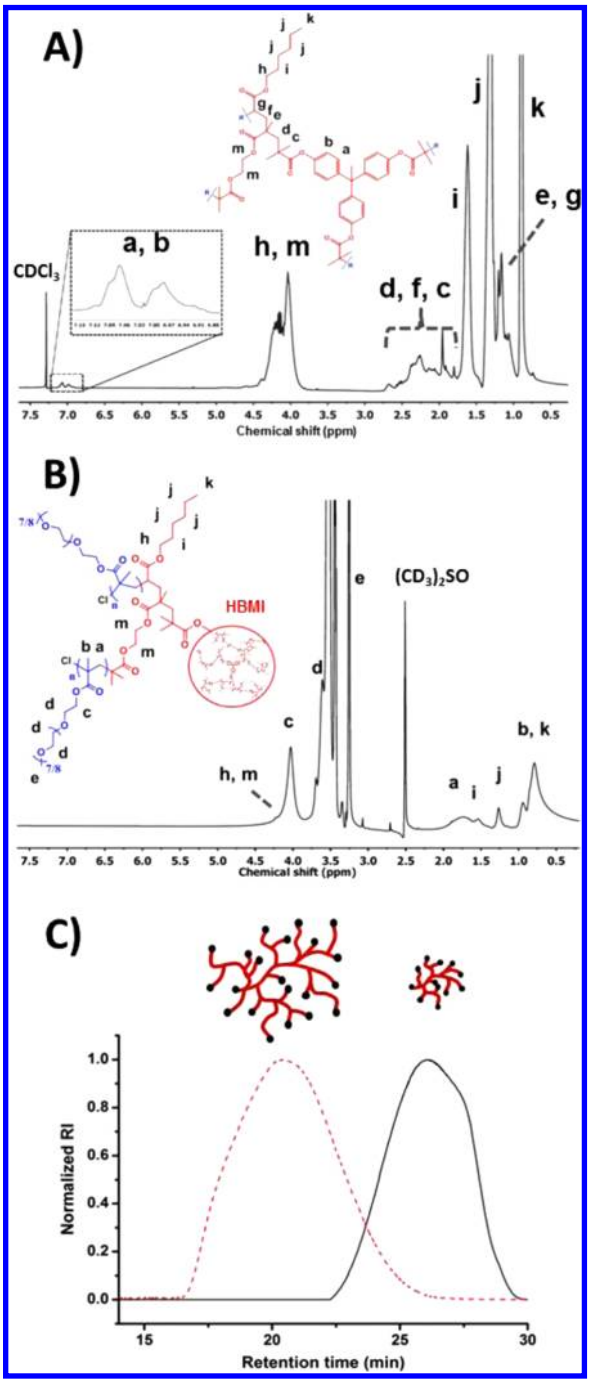

Figure 1. (A) ^{1}H NMR ($CDCl_3$) of HBMI-2. (B) ^{1}H NMR ($(CD_3)_2SO$) of HBDLP-5. (C) SEC traces of the two synthesized hyperbranched macroinitiators; HBMI-1 (solid black) and HBMI-2 (dashed red).

corresponding to the BBEMA (m) and HA (h) methylenes ($-O-CH_2-$) are clearly visible at 3.7−4.5 ppm. Further, at 0.8, 1.4, and 1.6 ppm peaks of the aliphatic protons of HA are observed. An additional advantage of using TBBPE in the reaction, in parallel to its potential reduction of the polymer molecular weight distribution, is the characteristic aromatic protons visible in the ^{1}H NMR around 7 ppm. The average compositions of the HBMIs (Table 1) is assessed from the appropriate integrals, and found to be in reasonable agreement with the monomers feed ratios taking into account experimental errors.

The HBMIs were also analyzed by SEC with DMF as the mobile phase (Table 1), even though it is well-known that SEC underestimates the molecular weight of hyperbranched polymers. The SEC traces for HBMI-1 and HBMI-2 are shown in Figure 1C, and the difference in elution time corroborates that there is a clear difference in hydrodynamic volume between the two HBMIs, as targeted. The molecular weights for HBMI-1 and HBMI-2 are determined by SEC to 3600 and 6100 g mol^{-1} respectively. Further, the HBMIs molecular weight dispersities ($Đ_M$, Table 1) are reasonable considering that the macroinitiators are hyperbranched polymers synthesized employing SCV(C)P, and comparable to similar studies.[57−59]

As simple as the syntheses of the HBMIs are, their characterization is challenging since there are several reactions with different kinetics involved in the formation of these polydisperse hyperbranched skeletons. Obviously, TBBPE has a significant effect on the final structure since the feed ratios of HA and BBEMA (4:1) are the same in HBMI-1 and HBMI-2, and yet the corresponding ^{1}H NMR and SEC are different. Also, the only way for a HBMI to comprise more than one TBBPE moiety is that it has been part of an undesired termination reaction (radical−radical coupling). In addition, if termination reactions had been frequent, a gel would have formed. Based on these two observations, and the fact that a CRP technique and a highly diluted system were used to suppress such coupling reactions, we find it reasonable to assume that the average HBMI molecule comprises one TBBPE moiety. Based on this assumption, it is possible to estimate the average degree of polymerization ($\overline{DP}$) of BBEMA and HA from ^{1}H NMR; the $\overline{DP}$'s of HBMI-1 and HBMI-2 were assessed to 49 and 346, respectively, which correspond to molecular weights of 10 000 and 61 000 g mol^{-1}. Assuming high end-group fidelity, the average number of Br per molecule can be gauged to 15 and 54 for HBMI-1 and HBMI-2, respectively.

The large differences between molecular weights determined by SEC and ^{1}H NMR is not unexpected; SEC is a relative technique relying on calibration with linear standards and is known to underestimate the molecular weight for hyperbranched polymers. ^{1}H NMR provides data for determination of number-average molecular weights but no evidence for connectivity. However, taking all aspects discussed above into account, we find it acceptable to utilize results from ^{1}H NMR for our further work.

Chain-Extension from the Hyperbranched Macroinitiators. In the second step of the synthesis, the hydrophobic HBMIs were utilized for chain-extension of linear hydrophilic polymers to form amphiphilic HBDLPs. As discussed earlier, OEGMAs have emerged as versatile alternatives for PEGylation. In this work we therefore chain-extend the HBMIs with varying lengths of OEGMA-based polymers to produce a library of HBMI-P(OEGMA) polymers (HBDLPs 1−5 in Table 2, Scheme 1, path A).

The polymerizations were conducted under conventional ATRP conditions, utilizing the active halide end-groups of the HBMIs, mediated by a 2,2-bipyridyl/Cu(I)Cl/Cu(II)Cl_2 system. Highly diluted toluene solutions were used as the reaction medium to avoid undesired irreversible coupling reactions when approaching high molecular weights, and the reactions were allowed to run to approximately 50% conversion. By aiming at different degrees of polymerization in the reactions

dx.doi.org/10.1021/bm5003637 | Biomacromolecules 2014, 15, 2235−2245

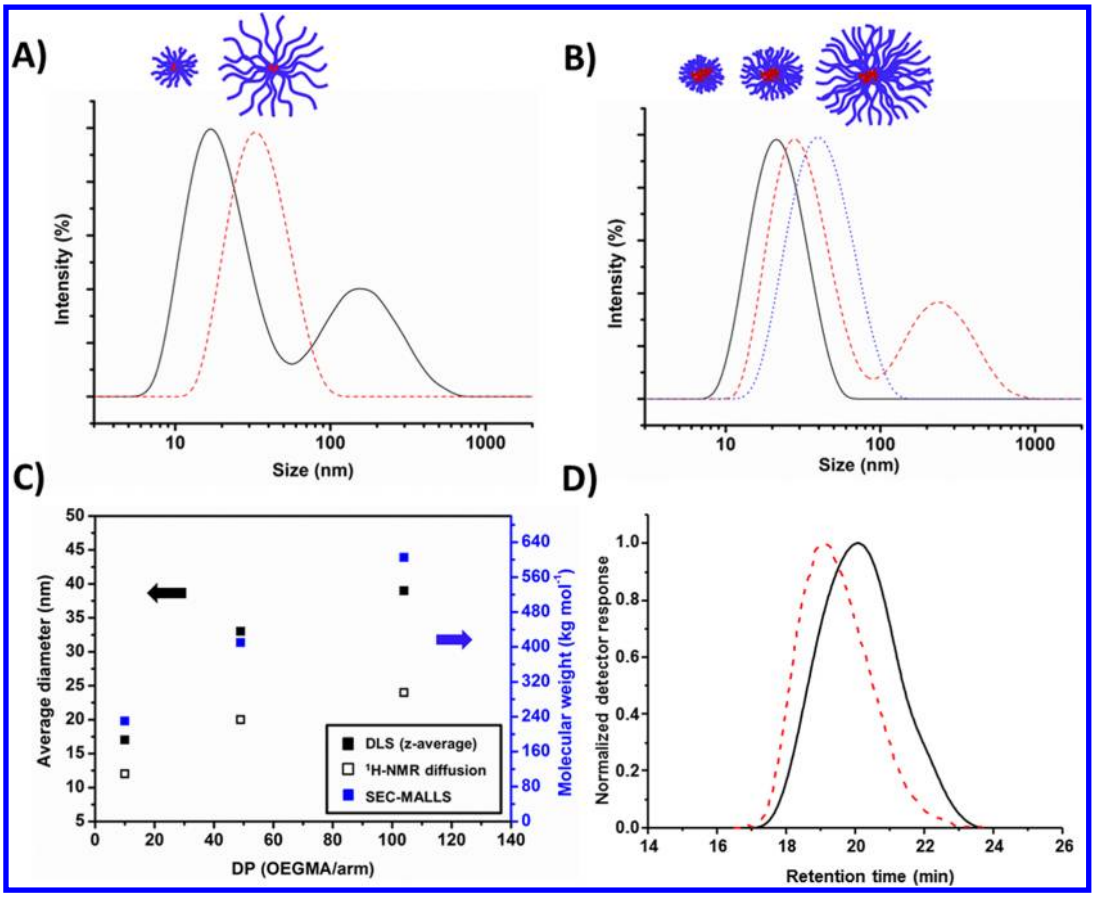

Figure 2. Hydrodynamic diameter distributions (intensity average) of the hyperbranched dendritic-linear polymers determined by DLS in PBS solution: (A) HBDLP-1 (solid black), HBDLP-2 (dashed red); (B) HBDLP-3 (solid black), HBDLP-4 (dashed red), HBDLP-5 (dotted blue). (C) Average diameter (DLS and NMR-d) and absolute molecular weight (SEC-MALLS) of HBDLP (HBDLP 3−5, Table 2) nanoparticles as a function of $\overline{DP}$ of the P(OEGMA) extensions. (D) Refractive index (solid black) and light scattering (dashed red) response as a function of retention time from SEC-MALLS of HBDLP-5 in H_2O (10 mM NaOH).

initiated from either HBMI-1 or HBMI-2, HBDLPs (HBDLP 1−5) of increasing hydrophilic extensions were achieved and analyzed with ^{1}H NMR, SEC, and SEC-MALLS (Table 2). Based on the discussion in the previous section, HBMI-2 has approximately 4 times more end-groups available for chain-extension, and should result in an amphiphilic HBDLP with a higher number of linear hydrophilic stabilizing arms, as compared to HBMI-1. A typical ^{1}H NMR of HBDLP-5, acquired in $(CD_3)_2SO$, is presented in Figure 1B. Characteristic peaks corresponding to the ethylene glycol segments (c and d) and methyl ethers (e) of P(OEGMA) are visible at 3.35−4.05 ppm. In addition, the methylene protons from HA in the HBMI (i and j) are still clearly visible at 1.27 and 1.54 ppm, demonstrating the successful formation of HBDLPs.

The $\overline{DP}$'s reported in Table 2 are calculated from ^{1}H NMR conversions based on the assumption discussed earlier, of growing arms from HBMI-1 and HBMI-2 to be 15 and 54, respectively. Most importantly, they illustrate that there is a clear difference between the HBDLPs synthesized from the same HBMI. SEC results in DMF, an expected good solvent for the HBDLPs, confirming the trend from ^{1}H NMR of increasing molecular weight of the HBDLPs with increasing length of the P(OEGMA) arms. For example, HBDLP-3 and HBDLP-5 with $\overline{DP}_{OEGMA/arm}$ of 10 and 104, assessed from NMR, show molecular weights from SEC of 28 and 153 kg mol^{-1}, respectively. However, it should be noted that the molecular weights are not absolute values; most likely the values are widely underestimated due to the complex architecture of the polymers. Furthermore, the chain-extension reactions proved to proceed in a controlled manner resulting in polymers with reasonably uniform SEC traces (Figure S1) and low molecular weight dispersities ($Đ_M$ = 1.3−1.7). The molecular weights of the HBDLPs were further analyzed by SEC-MALLS in aqueous solution. The differential index of refraction (dn/dc) of each HBDLP was determined (Figure S6), and employed to assess the absolute molecular weight (Table 2). The molecular weights from SEC-MALLS are higher (100−600 kg mol^{-1}) than from conventional SEC, but still presents the same trend of increasing molecular weights with increasing length of the P(OEGMA) segment as discussed earlier. However, it is important to keep in mind that SEC-MALLS, due to experimental limitations, were performed in aqueous solution, which for the complex amphiphilic structure of the HBDLPs may cause interpolymer association. Indications of such association can be seen in the refractive index distributions for some of the HBDLPs from SEC-MALLS reported in Figure 2D and the Supporting Information (Figure S7).

Recently, our group[43] as well as others[51,59−63] have suggested that incorporation of fluorinated monomers into the hydrophilic domain of polymer NPs is an interesting approach to enable potential diagnostic delivery systems. Therefore, to demonstrate the versatility of our polymer platform, we also evaluated the possibility to chain-extend HBMI-2 with a more

dx.doi.org/10.1021/bm5003637 | Biomacromolecules 2014, 15, 2235−2245

Table 2. Molecular Properties of the Prepared Hyperbranched Dendritic-Linear Polymers (HBDLPs) and Their Corresponding Nanoparticles

polymer	name[a]	macroinitiator	$\overline{DP}$/arm[b]	$M_{n,\,RI}$[d] (kg mol^{-1})	$M_{n,\,LS}$[e] (kg mol^{-1})	$Đ_M$[d]	$D_{h,\,number}$[f] (nm)	$D_{h,\,volume}$[f] (nm)	$D_{h,\,intensity}$[f] (nm)	$D_{h,\,Z}$[f] (nm)	$D_{diffusion}$[h] (nm)
HBDLP-1	$(HBMI\text{-}P(OEGMA))_{103k}$	HBMI-1	10	28	103	1.7	10 ± 1	13 ± 1	18 ± 1[g]	21 ± 2	10 ± 3
HBDLP-2	$(HBMI\text{-}P(OEGMA))_{473k}$	HBMI-1	116	132	473	1.5	18 ± 1	24 ± 1	37 ± 1	32 ± 1	20 ± 6
HBDLP-3	$(HBMI\text{-}P(OEGMA))_{230k}$	HBMI-2	10	28	230	1.3	11 ± 1	14 ± 1	20 ± 2	17 ± 2	12 ± 3
HBDLP-4	$(HBMI\text{-}P(OEGMA))_{410k}$	HBMI-2	49	81	410	1.5	16 ± 1	23 ± 2	34 ± 5[g]	33 ± 6	20 ± 5
HBDLP-5	$(HBMI\text{-}P(OEGMA))_{605k}$	HBMI-2	104	153	605	1.6	21 ± 1	30 ± 2	46 ± 1	39 ± 1	24 ± 6
HBDLP-6	$(HBMI\text{-}P(OEGMA\text{-}co\text{-}TFEMA\text{-}co\text{-}MAA))_{287k}$	HBMI-2	50[c]	51	287	1.6	12 ± 2	18 ± 2	32 ± 3[g]	37 ± 3	11 ± 4

[a]HBMI-P(OEGMA)$_x$, where x denotes the absolute molecular weight assessed by SEC-MALLS. [b]Theorethical $\overline{DP}$/arm assessed by ^{1}H NMR. [c]$\overline{DP}$/arm of (OEGMA-*co*-TFEMA-*co*-MAA) (molar ratio 14:26:10) assessed by ^{1}H NMR. [d]Apparent number-average molecular weight determined by SEC with DMF as eluent and calibrated with linear PMMA standards. [e]Absolute number-average molecular weight determined by SEC-MALLS in aqueous solution (1.50 mg mL^{-1}, 10 mM NaOH). [f]mean nanoparticle diameters (number, volume, intensity and z-averages) determined by DLS in PBS solution (1.25 mg mL^{-1}). Each size result, presented as diameter ± st.dev, is an average of four individual samples where each sample is an average of 10 subsequent runs. All polymers displayed a very small amount (1−4 intensity %) of aggregates of around 4000 nm in the intensity averages. [g]20−30 intensity % of aggregates of 250−300 nm visible. [h]Determined by ^{1}H NMR diffusion in PBS solution (1.25 mg mL^{-1}, η (25 °C) = 0.9 mPa s[64]) employing the Stokes−Einstein eq (eq S1). The average mean diameters and standard deviations were calculated from the average of two distributions (signal at 3.7 and 3.4 ppm) for each sample, except for HBDLP-1, where experimental noise did not allow accurate regression analysis for the signal at 3.4 ppm.

complex linear copolymer. HBDLP-6 was successfully synthesized by a two-step procedure, as illustrated in Scheme 1 (path B1 + B2). In the initial step, the polymerization initiated from HBMI-2 was conducted utilizing similar reaction conditions as the chain-extensions to form HBDLP 1−5, however, instead by utilizing the three commercially available vinyl monomers OEGMA, TFEMA, and *t*-BMA (Scheme 1, path B1). The ^{1}H NMR ($CDCl_3$) of the resulting polymer, HBMI-P(OEGMA-*co*-TFEMA-*co*-*t*BMA), is shown in Figure S3A, and from this the molar ratio of the linear polymer extension was calculated to be 28%, 52%, and 20% of OEGMA, TFEMA, and *t*-BMA, respectively. In the second step (Scheme 1, path B2), the *tert*-butyl groups were removed to form MAA residues by a facile deprotection procedure employing TFA, thus resulting in HBDLP-6 (Table 2 and Figure S3B). Despite the high fluorine content of HBDLP-6, it shows good water solubility (>20 mg mL^{-1}). However, it was found crucial that the polymer was stored under inert atmosphere, or else strong hydrogen bonds were formed and hampered dissolution in aqueous solution without the addition of base. Furthermore, the incorporation of fluorine atoms into the polymer exterior was demonstrated by ^{19}F-NMR in D_2O, where the chemically equivalent ^{19}F atoms of TFEMA give rise to a singlet peak at 2.15 ppm relative to a TFA reference (Figure S4).

Nanoparticle Formation and Characterization. The library of synthesized HBDLPs was evaluated as potential unimolecular NPs in aqueous PBS solution. The extension of highly hydrophilic segments from the hydrophobic HMBI core is proposed to facilitate stabilization of the polymers in three dimensions. Consequently, the architecture, reasonable high molecular weight, and an appropriate hydrophobic/hydrophilic ratio of the HBDLPs may enable formation of discrete unimolecular micelles, without any self-assembly, which traditionally is the case for amphiphilic block copolymer micelles. The HBDLPs were organized into core−shell type NPs by a solvent to nonsolvent procedure (from CH_2Cl_2 to PBS), more precisely described in the Experimental Section. To ensure the eligibility of the NP formation procedure, NPs formed by long time dissolution in PBS were also analyzed by DLS with very similar results. The characteristics of the NPs were then evaluated by DLS, ^{1}H NMR self-diffusion (NMR-d), SEC-MALLS, and TEM, and are shown in Table 2. Results of the average hydrodynamic diameters from DLS (1.25 mg mL^{-1} in PBS), assuming that all species are spherical in shape, indicates that the HBDLPs form NPs with mean diameters (z-average) between 17 and 39 nm. However, it is important to keep in mind that these values are means of a distribution, and some of the NPs (HBDLP 1, 4, and 6 in Table 2) display a small quantity of aggregated structures of 250−300 nm in diameter for the intensity distributions (Figure 2A and 2B). The formation of aggregates suggests that the hydrophilic/hydrophobic balance of the reported HBDLPs plays a crucial role to the NP stability. Noticeably, the NPs are uniform with similar values for the four diameter averages (number, volume, and intensity, and z-average). Further, analysis of the NPs by DLS, without filtration prior to the measurement, revealed that all NPs displayed 1−4 intensity % of large (around 4000 nm) particles, indicating aggregates or dust particles in addition to the intensity averages reported in Table 2. This indicates that even though most of the HBDLPs almost exclusively form stable individual NPs, some interparticle association may occur to a small extent. By comparing the NPs formed by HBDLP-1 and HBDLP-3, having different size of the hyperbranched core, but similar length of P(OEGMA)/arm, there is a small difference in NP size from DLS, thus indicating that the core has a minor influence on the overall NP size. The hydrophobic core is most probably collapsed in the PBS solution, only slightly contributing to the size, in contrast to the more extended state of the soluble P(OEGMA) exterior. Very interestingly, for both groups of HBDLPs; 1−2 and 3−5, a clear correlation between the length of the P(OEGMA) extension and the average size of the NPs can be seen (Table 2). For example, by increasing the $\overline{DP}_{OEGMA/arm}$ from 10 (HBDLP-3) to 104 (HBDLP-5), the average diameter of the NPs were increased from 17 to 39 nm. Furthermore, the NPs were analyzed by NMR-d, and for all HBDLPs it was found that the NMR signals in the NMR spectra, except for the water signal, displayed identical diffusion decay, and could evidently be assigned to the same molecule. The self-diffusion coefficient distribution was correlated to the NP diameter distribution by the Stokes−Einstein eq (eq S1), and the average mean diameters confirmed the trend seen from DLS with increasing particle diameters with increasing P(OEGMA) extension (Figure 2C). Although, the diameters determined by NMR-d typically are

lower in comparison to DLS, the two techniques show good correlation. This difference is expected since DLS to some extent overestimates larger objects, while NMR-d rather does the same for smaller specimen.[65] Conclusively, DLS and ^{1}H NMR diffusion indicates that the proposed HBDLPs can be employed to form NPs with a tunable size, and therefore implies a potential strategy to design unimolecular micelles.

The NP properties in aqueous solution were further evaluated by SEC-MALLS (10 mM NaOH). The results reported in Table 2 clearly states that the NPs formed have high molecular weights (100−600 kg mol^{-1}), and that the increase in molecular weight of the NPs correlates well with the trend of increasing NP diameters determined by DLS and NMR-d (Figure 2C). However, the RI distribution curves from SEC-MALLS (Figures 2D and S6) reveals that the NPs originating from the small HBMI (HBDLP-1 and HBDLP-2), and from the larger HBMI with short P(OEGMA) segments (HBDLP), are not completely individually stabilized. The bimodality in the RI signals indicates that the HBDLPs to some extent aggregates. However, when comparing these results to DLS and NMR-d data, it is important to keep in mind the difference in solvent since SEC-MALLS equipment were not available for analysis in PBS. When reaching higher molecular weight and increasing P(OEGMA)-to-HBMI ratio (HBDLP-4 and HBDLP-5), the uniform RI distributions suggests that the HBDLPs form significantly more stable NPs, which is indicative of the fact that unimolecular micelles are achieved.

Since both DLS and NMR-d estimate the NP size as a function of its diffusivity in solution by the Stokes−Einstein equation, assuming a spherical shape, their morphology and size were further evaluated by TEM (Figures 3 and S7). Figure 3

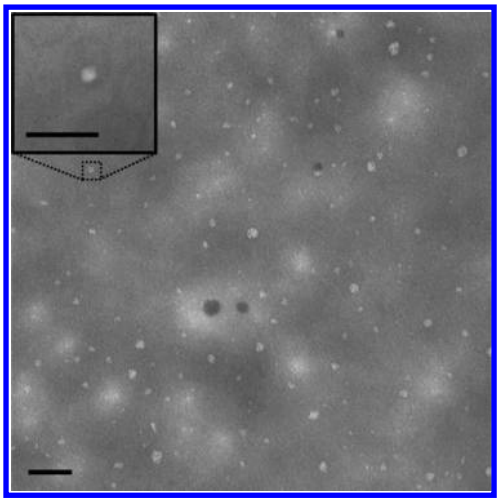

Figure 3. TEM micrograph of HBDLP-5 NPs at 22K magnification. Inset: 44K magnification. Scale bars are 100 nm.

shows a representative TEM micrograph (HBDLP-5) observed at 22K magnification (inset: 44K magnification). It can be seen that the NPs formed have a fairly uniform size distribution and are spherical in shape, thus suggesting that the DLS and NMR-d assumption of a spherical structure is correct. The NP sizes measured by TEM are within the interval 10−20 nm and are assessed as an average of 30−180 particles within the same micrograph. The somewhat smaller NP sizes determined by TEM compared to DLS and NMR-d, are expected since with TEM the NPs are analyzed in the dry state, while DLS and NMR-d are performed in solution, and hence the NPs shells are swollen.

In the composition of HBDLP-6, as much as 52 mol % of the OEGMA monomers in the hydrophilic NP domain is replaced by the less water-soluble TFEMA monomers. As reported in Table 2, the NPs from HBDLP-6 show comparable diameter averages to its 100% P(OEGMA)-extended analogue (HBDLP-4). Additionally, similar to HBDLP-4, the fluorine-containing HBDLP-6 NPs show some extent of aggregation in the DLS intensity averages that is not seen for the other HBDLPs synthesized from HBMI-2. This indicates that the hydrophilic/hydrophobic ratio may be a potential cause of the aggregation.

Cell-Based Tests of the Hyperbranched Dendritic-Linear Polymers. To evaluate the potential of the NPs as therapeutic delivery systems, an initial biological evaluation was conducted. First, the cytotoxicity of HBDLPs 1−6 to four different cell lines was evaluated. The NPs were incubated individually at varying concentrations (0.01−100 μg mL^{-1}) with the three human breast cancer cell lines, MDA-MB-231, MDA-MB-468, and MCF-7, as well as with the mouse macrophage cell line RAW 264.7. After 72 h of incubation, the mitochondrial activity of the cells was evaluated by an MTT assay, and the results are seen in Figures 4 and S9. For the five

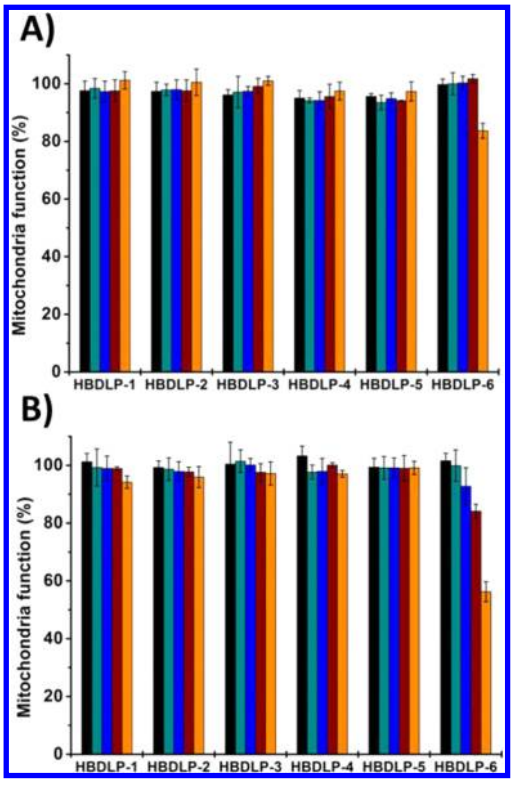

Figure 4. Effect of the nanoparticles to the mitochondria function of (A) breast cancer cell line MDA-MB-231 and (B) mouse macrophage cell line RAW 264.7, after 72 h of incubation at varying concentrations (0.01 μg mL^{-1} − black; 0.1 μg mL^{-1} − green; 1 μg mL^{-1} − blue; 10 μg mL^{-1} − red; 100 μg mL^{-1} − orange).

P(OEGMA)-extended HBDLPs (HBDLP 1−5), no significant reduction in mitochondria function were found to any of the cell lines within this concentration range. However, HBDLP-6 to some extent showed a reduction in mitochondria function to the cell lines. This was most pronounced at high polymer concentrations for the MCF-7 and RAW 264.7 cell lines, where the mitochondrial activity was reduced to ca. 60% at the highest polymer concentration. This viability reduction may be an effect of

dx.doi.org/10.1021/bm5003637 | Biomacromolecules 2014, 15, 2235−2245

remaining traces of copper from the synthesis. Although, all polymers are purified with extensive EDTA dialysis, the strong hydrogen bonds earlier mentioned for HBDLP-6 may restrict a complete copper removal. Further, the HBDLPs abilities to encapsulate and deliver small molecular therapeutic doxorubicin (DOX) were evaluated in vitro. NPs of HBDLP 1, 3, 4, and 5 were successfully loaded with DOX, and their effect to the cell line MDA-MB-468 was evaluated. In vitro drug release of the DOX-NPs demonstrated a slower release profile compared to free DOX (Figure S10), and about 60% of the DOX was released from the NPs within 10 h. In addition, all the DOX-loaded NPs demonstrated a dose-dependent efficacy to the MDA-MB-468 cells (Figure S11). In order to study whether the DOX-NPs can deliver drugs to the cells, confocal microscopy was applied to observe DOX localization in the cell line MDA-MB-468. According to Figure S12 free DOX is taken up by the cells within a short period (2 h), and mainly accumulated close or in the nuclei. DOX-NPs proved to also deliver DOX into the cells, and the DOX is localized to the cell nuclei and in the cytoplasm. Compared to the free drug, the DOX delivery from the NPs occur more gradually, and after 24 h, more DOX was accumulated around the nuclei (blue), indicated by the more purple (colocalization) and red (DOX) color in the merged pictures.

CONCLUSIONS

In this study, PEGylated, hyperbranched dendritic-linear polymers (HBDLPs) were successfully synthesized and evaluated as potential unimolecular micelles. The amphiphilic HBDLPs were synthesized via a versatile two-step procedure. Initially, hydrophobic hyperbranched macroinitiators (HBMI) were produced employing self-condensing vinyl (co)polymerization (SCV(C)P) utilizing atom transfer radical polymerization (ATRP). Subsequently, the active end-groups were exploited to chain-extend the HBMIs with linear, hydrophilic poly(ethylene glycol) methacrylate (P(OEGMA)) segments via ATRP, forming high molecular weight amphiphilic HBDLPs. A library of high molecular weight polymers, with either different size of the hyperbranched segment, or varying length of the linear segments was afforded. The corresponding HBDLP NPs were extensively characterized in solution by DLS, ^{1}H NMR self-diffusion, and SEC-MALLS, as well as by TEM in the dry state. All HBDLPs proved to form predominantly stable and spherical NPs, and provided for opportunities to tailor the NP dimensions, from 17 to 39 nm, by the polymer architecture and hydrophobic/hydrophilic ratio. The size of the dendritic segment was found to have minor influence on the final NP diameter, while the length of the P(OEGMA) segments affected the size to a larger extent. This corroborates that the hydrophobic NP interior is in a collapsed, dense state, in aqueous environment, surrounded by a more extended hydrophilic exterior. Analysis by SEC-MALLS showed that the NPs formed have high absolute molecular weights (100−600 kg mol^{-1}), and the increase in molecular weight correlated well to the increase in NP diameter afforded by DLS and NMR-d. SEC-MALLS further proved some aggregation of the NPs from the HBDLPs with too small dendritic segment, or too low hydrophilic/hydrophobic ratio; however, the highest molecular weight HBDLP showed promising properties of stable discrete unimolecular micelles. The neat NPs proved to be nontoxic to three breast cancer cell lines and one mouse macrophage cell line in the concentration range tested (<100 μg mL^{-1}). Further, the NPs could be loaded with the molecular therapeutic doxorubicin and showed a slower release profile compared to free doxorubicin, as well as dose-dependent toxicity to breast cancer cells. In addition, one of the HBMIs was successfully chain-extended with a fluorine-containing copolymer, thus demonstrating the versatility of the HBDLP platform by introducing additional functionality to the NPs. Conclusively; SCV(C)P-ATRP is a promising approach to design high molecular weight HBDLPs with a great designer freedom, due to the versatility of controlled radical polymerization techniques. Furthermore, the beneficial architecture and conceivable high molecular weight of such polymers can be tailored in order to enable unimolecular micelles, with applicability, for instance, in drug delivery applications.

ASSOCIATED CONTENT

Supporting Information

Size distributions (SEC, DLS, ^{1}H NMR self-diffusion, SEC-MALLS), ^{1}H NMR spectra, dn/dc plots, TEM images, and cell viability, in vitro DOX release, and localization studies. This material is available free of charge via the Internet at http://pubs.acs.org

AUTHOR INFORMATION

Corresponding Author

*E-mail: mavem@kth.se.

Author Contributions

The manuscript was written through contributions of all authors. All authors have given approval to the final version of the manuscript.

Notes

The authors declare no competing financial interest.

ACKNOWLEDGMENTS

Funding support by the Swedish Research Council (VR), grants 2011-3720 and 2009-3259, are greatly acknowledged. NMR self-diffusion experiments were carried out at the Swedish NMR Centre.

REFERENCES

(1) Ferrari, M. *Nat. Rev. Cancer* **2005**, *5* (3), 161−171.
(2) Elsabahy, M.; Wooley, K. L. *Chem. Soc. Rev.* **2012**, *41* (7), 2545−2561.
(3) Otsuka, H.; Nagasaki, Y.; Kataoka, K. *Adv. Drug Delivery Rev.* **2003**, *55* (3), 403−419.
(4) Owens, D. E., 3rd; Peppas, N. A. *Int. J. Pharm.* **2006**, *307* (1), 93−102.
(5) Kataoka, K.; Kwon, G. S.; Yokoyama, M.; Okano, T.; Sakurai, Y. *J. Controlled Release* **1993**, *24* (1−3), 119−132.
(6) Blanazs, A.; Armes, S. P.; Ryan, A. J. *Macromol. Rapid Commun.* **2009**, *30* (4−5), 267−277.
(7) Discher, D. E.; Eisenberg, A. *Science* **2002**, *297* (5583), 967−973.
(8) Thurmond, K. B., II; Kowalewski, T.; Wooley, K. L. *J. Am. Chem. Soc.* **1996**, *118* (30), 7239−7240.
(9) Astruc, D.; Boisselier, E.; Ornelas, C. *Chem. Rev.* **2010**, *110* (4), 1857−1959.
(10) Lee, C. C.; MacKay, J. A.; Fréchet, J. M. J.; Szoka, F. C. *Nat. Biotechnol.* **2005**, *23* (12), 1517−1526.
(11) Wang, Y.; Grayson, S. M. *Adv. Drug Delivery Rev.* **2012**, *64* (9), 852−865.
(12) Medina, S. H.; El-Sayed, M. E. H. *Chem. Rev.* **2009**, *109* (7), 3141−3157.
(13) Lee, C. C.; Gillies, E. R.; Fox, M. E.; Guillaudeu, S. J.; Fréchet, J. M.; Dy, E. E.; Szoka, F. C. *Proc. Natl. Acad. Sci. U. S. A.* **2006**, *103* (45), 16649−16654.
(14) Aulenta, F.; Hayes, W.; Rannard, S. *Eur. Polym. J.* **2003**, *39* (9), 1741−1771.
(15) Gitsov, I. *J. Polym. Sci., Part A: Polym. Chem.* **2008**, *46* (16), 5295−5314.

(16) Gillies, E.; Fréchet, J. *Drug Discovery Today* **2005**, *10* (1), 35−43.
(17) Flory, P. J. *J. Am. Chem. Soc.* **1952**, *74*, 2718−2723.
(18) Fréchet, J. M. J.; Henmi, M.; Gitsov, I.; Aoshima, S.; Leduc, M. R.; Grubbs, R. B. *Science* **1995**, *269* (5227), 1080−1083.
(19) Wang, J.-S.; Matyjaszewski, K. *J. Am. Chem. Soc.* **1995**, *117* (20), 5614−5615.
(20) Kato, M.; Kamigaito, M.; Sawamoto, M.; Higashimura, T. *Macromolecules* **1995**, *28* (5), 1721−1723.
(21) Chiefari, J.; Chong, Y. K.; Ercole, F.; Krstina, J.; Jeffery, J.; Le, T. P. T.; Mayadunne, R. T. A.; Meijs, G. F.; Moad, C. L.; Moad, G.; Rizzardo, E.; Thang, S. H. *Macromolecules* **1998**, *31* (16), 5559−5562.
(22) O'Brien, N.; McKee, A.; Sherrington, D. C.; Slark, A. T.; Titterton, A. *Polymer* **2000**, *41* (15), 6027−6031.
(23) He, T.; Adams, D. J.; Butler, M. F.; Cooper, A. I.; Rannard, S. P. *J. Am. Chem. Soc.* **2009**, *131* (4), 1495−1501.
(24) Weaver, J. V. M; Williams, R. T.; Royles, B. J. L.; Findlay, P. H.; Cooper, A. I.; Rannard, S. P. *Soft Matter* **2008**, *4* (5), 985−992.
(25) Hawker, C. J.; Fréchet, J. M. J.; Grubbs, R. B.; Dao, J. *J. Am. Chem. Soc.* **1995**, *117* (43), 10763−10764.
(26) Gaynor, S. G.; Edelman, S.; Matyjaszewski, K. *Macromolecules* **1996**, *29* (3), 1079−1081.
(27) Yan, D.; Müller, A. H. E.; Matyjaszewski, K. *Macromolecules* **1997**, *30* (23), 7024−7033.
(28) Al-Muallem, H. A.; Knauss, D. M. *J. Polym. Sci., Part A Polym. Chem.* **2000**, *39* (1), 152−161.
(29) Mori, H.; Müller, A. H. E.; Simon, P. F. W. *Hyperbranched Polym.* **2011**, 139−174.
(30) Mori, H.; Seng, D. C.; Lechner, H.; Zhang, M.; Müller, A. H. E. *Macromolecules* **2002**, *35* (25), 9270−9281.
(31) Prabaharan, M.; Grailer, J. J.; Pilla, S.; Steeber, D. A.; Gong, S. *Biomaterials* **2009**, *30* (16), 3009−3019.
(32) Li, X.; Qian, Y.; Liu, T.; Hu, X.; Zhang, G.; You, Y.; Liu, S. *Biomaterials* **2011**, *32* (27), 6595−6605.
(33) Liu, M.; Kono, K.; Fréchet, J. M. J. *J. Controlled Release* **2000**, *65* (1−2), 121−131.
(34) Walter, M. V.; Lundberg, P.; Hult, D.; Hult, A.; Malkoch, M. *Polym. Chem.* **2013**, *4* (9), 2680.
(35) Carlmark, A.; Hawker, C.; Hult, A.; Malkoch, M. *Chem. Soc. Rev.* **2009**, *38* (2), 352−362.
(36) Porsch, C.; Hansson, S.; Nordgren, N.; Malmström, E. *Polym. Chem.* **2011**, *2* (5), 1114−1123.
(37) Östmark, E.; Harrisson, S.; Wooley, K. L.; Malmström, E. E. *Biomacromolecules* **2007**, *8* (4), 1138−1148.
(38) Öberg, K.; Hed, Y.; Rahmn, I. J.; Kelly, J.; Löwenhielm, P.; Malkoch, M. *Chem. Commun.* **2013**, *49* (62), 6938−6940.
(39) Andrén, O. C. J.; Walter, M. V.; Yang, T.; Hult, A.; Malkoch, M. *Macromolecules* **2013**, *46* (10), 3726−3736.
(40) Östmark, E.; Nyström, D.; Malmström, E. *Macromolecules* **2008**, *41* (12), 4405−4415.
(41) Larsson, E.; Sanchez, C. C.; Porsch, C.; Karabulut, E.; Wågberg, L.; Carlmark, A. *Eur. Polym. J.* **2013**, *49* (9), 2689−2696.
(42) Walter, M. V.; Malkoch, M. *Chem. Soc. Rev.* **2012**, *41* (13), 4593−4609.
(43) Porsch, C.; Zhang, Y.; Östlund, Å.; Damberg, P.; Ducani, C.; Malmström, E.; Nyström, A. M. *Part. Part. Syst. Charact.* **2013**, *30* (4), 381−390.
(44) Wu, Z.; Zeng, X.; Zhang, Y.; Feliu, N.; Lundberg, P.; Fadeel, B.; Malkoch, M.; Nyström, A. M. *J. Polym. Sci., Part A: Polym. Chem.* **2012**, *50* (2), 217−226.
(45) Zeng, X.; Zhang, Y.; Nyström, A. M. *Biomacromolecules* **2012**, *13* (11), 3814−3822.
(46) Hed, Y.; Zhang, Y.; Andren, O. C. J.; Zeng, X.; Nyström, A. M.; Malkoch, M. *J. Polym. Sci., Part A: Polym. Chem.* **2013**, *51* (19), 3992−3996.
(47) Zeng, X.; Zhang, Y.; Wu, Z.; Lundberg, P.; Malkoch, M.; Nyström, A. M. *J. Polym. Sci., Part A: Polym. Chem.* **2012**, *50* (2), 280−288.
(48) Lutz, J.-F. *J. Polym. Sci., Part A: Polym. Chem.* **2008**, *46* (11), 3459−3470.
(49) Thomson, D. A. C.; Tee, E. H. L.; Tran, N. T. D.; Monteiro, M. J.; Cooper, M. A. *Biomacromolecules* **2012**, *13* (6), 1981−1989.
(50) Du, W.; Nyström, A. M.; Zhang, L.; Powell, K. T.; Li, Y.; Cheng, C.; Wickline, S. A.; Wooley, K. L. *Biomacromolecules* **2008**, *9* (10), 2826−2833.
(51) Thurecht, K. J.; Blakey, I.; Peng, H.; Squires, O.; Hsu, S.; Alexander, C.; Whittaker, A. K. *J. Am. Chem. Soc.* **2010**, *132* (15), 5336−5337.
(52) Tanner, J. E. *J. Chem. Phys.* **1970**, *52* (5), 2523−2526.
(53) Holz, M.; Weingaertner, H. *J. Magn. Reson.* **1991**, *92* (1), 115−125.
(54) Schulz, G. V. *Z. Phys. Chem.* **1939**, *B43*, 25−46.
(55) Matyjaszewski, K.; Miller, P. J.; Pyun, J.; Kickelbick, G.; Diamanti, S. *Macromolecules* **1999**, *32* (20), 6526−6535.
(56) Matyjaszewski, K.; Gaynor, S. G.; Kulfan, A.; Podwika, M. *Macromolecules* **1997**, *30* (17), 5192−5194.
(57) Hong, C.-Y.; Zou, Y.-F.; Pan, C.-Y. *Polym. Int.* **2003**, *52* (2), 257−264.
(58) Cheng, K.-C. *Polymer* **2002**, *44* (3), 877−882.
(59) Du, W. J.; Nyström, A. M.; Zhang, L.; Powell, K. T.; Li, Y. L.; Cheng, C.; Wickline, S. A.; Wooley, K. L. *Biomacromolecules* **2008**, *9* (10), 2826−2833.
(60) Du, W.; Xu, Z.; Nyström, A. M.; Zhang, K.; Leonard, J. R.; Wooley, K. L. *Bioconjugate Chem.* **2008**, *19* (12), 2492−2498.
(61) Wang, K.; Peng, H.; Thurecht, K. J.; Puttick, S.; Whittaker, A. K. *Polym. Chem.* **2013**, *4* (16), 4480.
(62) Ogawa, M.; Kataoka, H.; Nitahara, S.; Fujimoto, H.; Aoki, H.; Ito, S.; Narazaki, M.; Matsuda, T. *Bull. Chem. Soc. Jpn.* **2012**, *85* (1), 79−86.
(63) Ogawa, M.; Nitahara, S.; Aoki, H.; Ito, S.; Narazaki, M.; Matsuda, T. *Macromol. Chem. Phys.* **2010**, *211* (12), 1369−1376.
(64) Armstrong, J. K.; Wenby, R. B.; Meiselman, H. J.; Fisher, T. C. *Biophys. J.* **2004**, *87* (6), 4259−4270.
(65) Wassenius, H.; Löfroth, J.-E.; Nyden, M. *Starch/Staerke* **2006**, *58* (2), 66−81.